Journal of Power Sources 265 (2014) 140–148

Contents lists available at ScienceDirect

Journal of Power Sources

journal homepage: www.elsevier.com/locate/jpowsour

In-situ investigation of solid-electrolyte interphase formation on the anode of Li-ion batteries with Atomic Force Microscopy

Lixin Wang [a], Da Deng [a], Leonid C. Lev [b], Simon Ng [a,*]

[a] Department of Chemical Engineering and Materials Science, Wayne State University, USA
[b] Manufacturing Systems Research Lab, Warren Technical Center, General Motors Company, USA

HIGHLIGHTS

- In-situ AFM is used to study SEI formation on the surface of graphite Li-ion electrode.
- It is observed that SEI is composed of a top particle layer and a bottom insertion layer.
- A top particle layer and a second layer underneath the top layer were observed in SEI.
- A dynamic competition mechanism between two layers of SEI is proposed.

ARTICLE INFO

Article history:
Received 6 March 2014
Received in revised form
22 April 2014
Accepted 22 April 2014
Available online 30 April 2014

Keywords:
In-situ AFM
HOPG
Graphite
SEI
Lithium ion batteries

ABSTRACT

Solid-electrolyte interphase (SEI) formation at highly ordered pyrolytic graphite (HOPG) surface has been studied with in-situ AFM. The morphology and thickness of both the top particle layer of the SEI and the bottom layer of the SEI that was caused by lithium insertion were investigated. The formation mechanism of the SEI was proposed accordingly. Ex-situ FESEM and EDS were also used to analyze the composition of the electrode after cycling to confirm the proposed mechanism.

1. Introduction

In-situ Atomic Force Microscopy (AFM), as a powerful tool for investigating surface morphology, has found its way into the study of solid-electrolyte interphase (SEI) in Li-ion batteries in recent years. Several groups have reported their results on the SEI evolution on Sn electrode [1], silicon electrode [2,3], and carbon based materials studied by in-situ AFM [4–10]. Mechanisms have also been proposed to explain the phenomenon at the SEI during charge–discharge processes. For example, Inaba et al. observed that the basal surface of HOPG raises 1 nm at a discharge voltage of 1.1 V. They believe this hill-like raise is caused by the co-intercalation of solvated lithium ion due to the conductivity of the tested area [4]. The mechanism of the SEI formation is therefore proposed as two steps: firstly, the insertion of the solvated lithium ion into the basal plane; secondly, the direct decomposition of solvent to form a blister layer which prevents further solvent co-intercalation. The formation of the surface film on graphite composite electrodes was observed by Jeong et al. in an EC/DEC based electrolyte [7]. Instead of swelling at the basal plane, they observed the curling of the graphite flake edges at a discharge voltage below 1.4 V. Significant morphology changes were observed after the voltages steps reduction due to the large amount of precipitations on the surface.

These studies [1–10] show the effectiveness of in-situ AFM to study SEI, and the role of SEI formation during charging and discharging Li-ion batteries. However, the effect of solvent decomposition products on lithium ion insertion, the thickness changes, and the compositions of the SEI during the cycling have not been fully elucidated. A better understanding of the formation and evolution of SEI during charge and discharge will provide valuable data to determine the role of SEI in the failure mechanism of Li-ion batteries. In addition, it might provide some insight on how to

* Corresponding author. Tel.: +1 313 577 3805; fax: +1 313 577 8171.
E-mail address: sng@wayne.edu (S. Ng).

http://dx.doi.org/10.1016/j.jpowsour.2014.04.113
0378-7753/

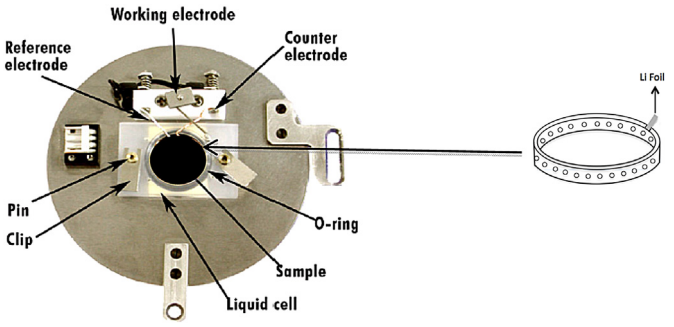

Fig. 1. Photo of liquid cell with electrochemistry setup.

optimize the SEI layer in a dynamic balance state, before it eventually becomes a complete insulator. Thus, storage and operating conditions can be controlled and optimized to extend battery life and improve performance.

In this report, a step-by-step evolution of both the solvent decomposition layer and the intercalation of solvated lithium ions, as well as the interactions between the two at different discharge voltages in the first charge–discharge cycle, are investigated. The thickness of the SEI is measured by scratching away both layers. A possible dynamic competition mechanism of the SEI formation has been proposed based on the experimental results. A HOPG plate is chosen as the electrode for the mechanism study due to the uniformity of its surface, more accurate thickness, easier operation of AFM probes on its smooth and renewable surface. A graphite composite electrode, which is more close to commercial Li-ion electrode, was studied followed by the studies of the HOPG surface. Very similar phenomenon has been found in the graphite composite electrode as well. The in-situ tested graphite composite samples are then characterized using ex-situ SEM and EDS to confirm the morphology and composition of the SEI layers.

2. Experiment

The experiments were performed in a liquid cell from Agilent technology with an insert to fix Li-strip in place as shown in Fig. 1 [11]. A 1.5 × 1.5 cm^{-2} square HOPG (ZYH grade, Momentive) was mounted at the bottom of the liquid cell. A lithium metal strip (0.2 × 5 cm, 99.9% pure, 0.75 mm thick, Alfa Aesar) was placed inside the insert around the wall of the liquid cell as the reference and counter electrode. The lithium strip contacted with the electrolyte through the round holes on the insert. 1.0 M $LiPF_6$ ethylene carbonate/dimethyl carbonate solution (1:1 volume ratio) was placed in the liquid cell sealed with an O-ring and a PTFE liquid cell frame. The liquid cell frame was pinned to the stainless steel sample holder by two pins to ensure the tightness. The AFM scanner was placed at the center of the liquid cell. The electrodes were then connected to the build-in electrochemical testing of the AFM system from the connector. The voltage range of 0.02–3.0 V was used in the electrochemical test with a 0.5 mV s^{-1} charge–discharge rate. All the operations were done inside a glove box filled with dry Ar gas to prevent oxidation and moisture contamination of the electrode materials and the electrolyte.

The graphite composite electrode was rinsed with EC/DMC (1:1) solution thoroughly and completely dried inside the grove box. Field emission scanning microscopy (FESEM) and energy dispersive X-ray spectrometer (JSM-7600F at 15 kV) were used to characterize the morphology and composition of the dry sample.

3. Results and discussion

3.1. Electrochemical testing

The electrochemical test is performed on the HOPG sample in the liquid cell described above. As shown in the cyclic voltammetry curve, redox current was observed when the discharge voltage is around 2.5 V. A redox peak at 0.95 V was observed in the first discharge process at the scan rate of 0.5 mV s^{-1}, indicating the occurring of a redox reaction. However, the peak disappeared after the eighth cycle, which indicates that the reactions responsible for the 0.95 V_{Li} peak are not reversible (Fig. 2).

3.2. SEI morphology evolution during the first charge–discharge cycle on the surface of HOPG

The morphology change of the HOPG surface was observed by AFM synchronously. Since the AFM probe and the cyclic voltammetry were performed at the same time, one AFM image shows a range of charging as indicated in Fig. 3. As shown in Fig. 3 a and b, there is slight topographical change on the HOPG surface between the discharge voltage of 3.0–1.65 V. Particles of about 100 nm at the interphase of the electrode/electrolyte start to form at a discharging

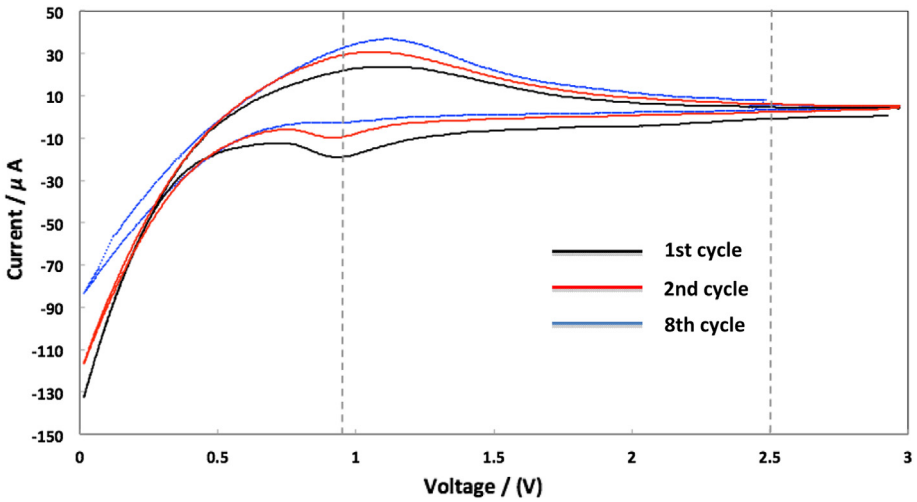

Fig. 2. Cyclic voltammogram of the graphite electrode with a scan rate of 0.5 mV s^{-1}.

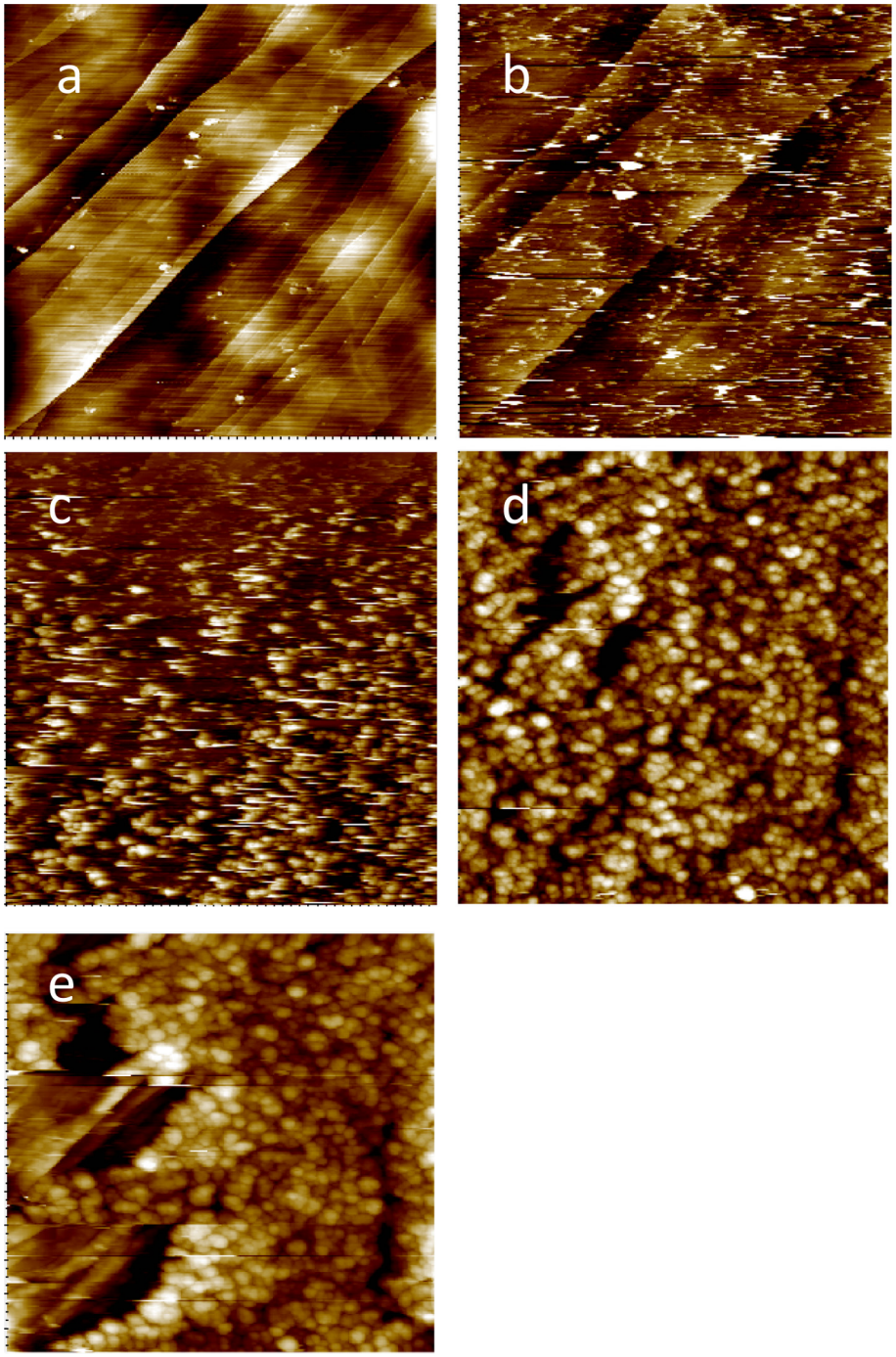

Fig. 3. AFM images of HOPG surface scanned at a synchronous discharge voltage range of a) 3.0–2.95 V; b) 1.7–1.65 V; c) 1.0–0.95 V; d) 0.5–0.45 V; e) 0.1–0.05 V. Scan area 25 μm^2.

voltage of 1.7 V. These particles are believed to be the decomposition products, such as lithium alkoxides, lithium alkyl carbonate and their polymerized compounds [12–15]. When the discharging voltage is lowered to around 0.95 V, a large amount of particles started to appear rapidly, which is correlated with the reduction peak around this voltage. It is clearly shown in Fig. 3c that particles grow intensely within the same scan from the top to the bottom. At the beginning, only a few particles can be observed (top part of Fig. 3c). With the scanning from the top to the bottom and charging voltage changes from 1.7 to 1.1 V, a large amount of particles appeared on the surface of HOPG as shown at the bottom part of Fig. 3c. The top particle layer of the SEI started to exfoliate at a lower voltage of around 0.5–0.02 V. The second layer can be seen underneath the particle layer, which appeared as strips as shown in the lower left corner of Fig. 3e. At the end of the first discharge process, the particles in the top layer grew to around 200 nm at 0.02 V.

In order to reveal the evolution of HOPG surface underneath the top particle layer, a 10 mV force is applied on the surface to remove the loose top particle layer during the first discharge process and preserve the bottom layer at the same time. As can be seen from Fig. 4b, the edge of the atomic steps shows swelling at a

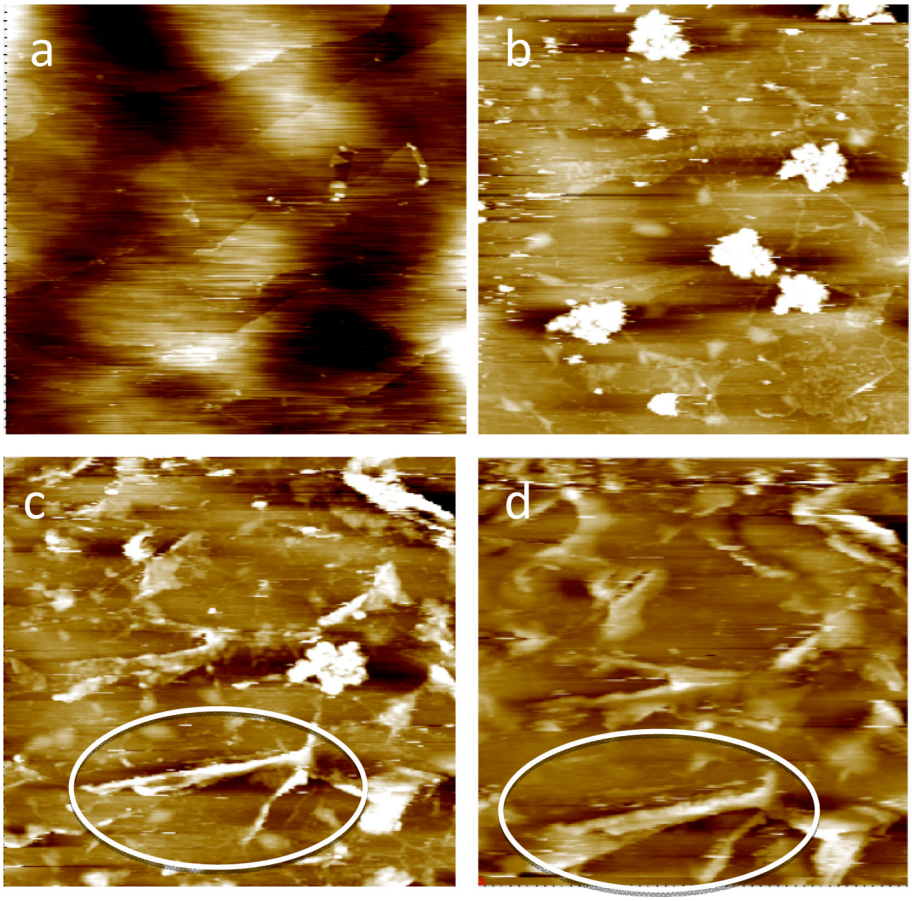

Fig. 4. AFM images of bottom SEI layer: a) pristine HOPG; b) discharge to 1.7 V; c) discharge to 0.5 V; d) discharge to 0.02 V. Scan area 25 μm^2.

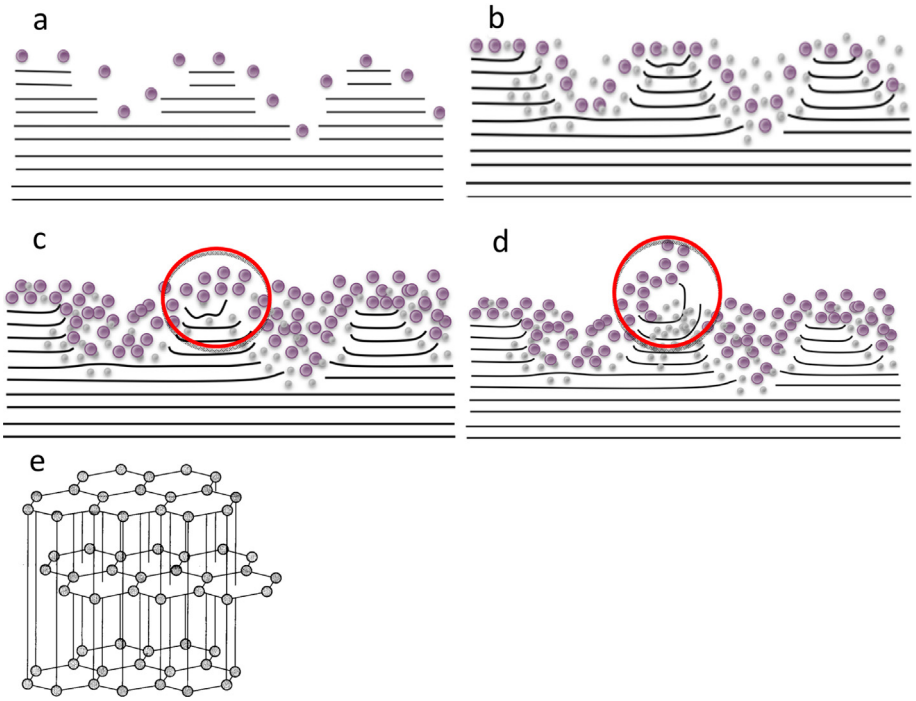

Fig. 5. Schematic of SEI evolutions during the first discharge process. a) The solvent decomposition product (purple dots) deposits at the surface of the graphite; b) the solvated lithium ions (gray dots) pass through the particle layer and intercalated into the graphite layer (black lines); c) solvent decomposition products accumulate at the surface when the lithium intercalation takes places; d) the displacement of the graphite layer caused by the lithium intercalation pushes the top particle layer off the HOPG surface; e) schematic of graphite. (For interpretation of the references to color in this figure legend, the reader is referred to the web version of this article.)

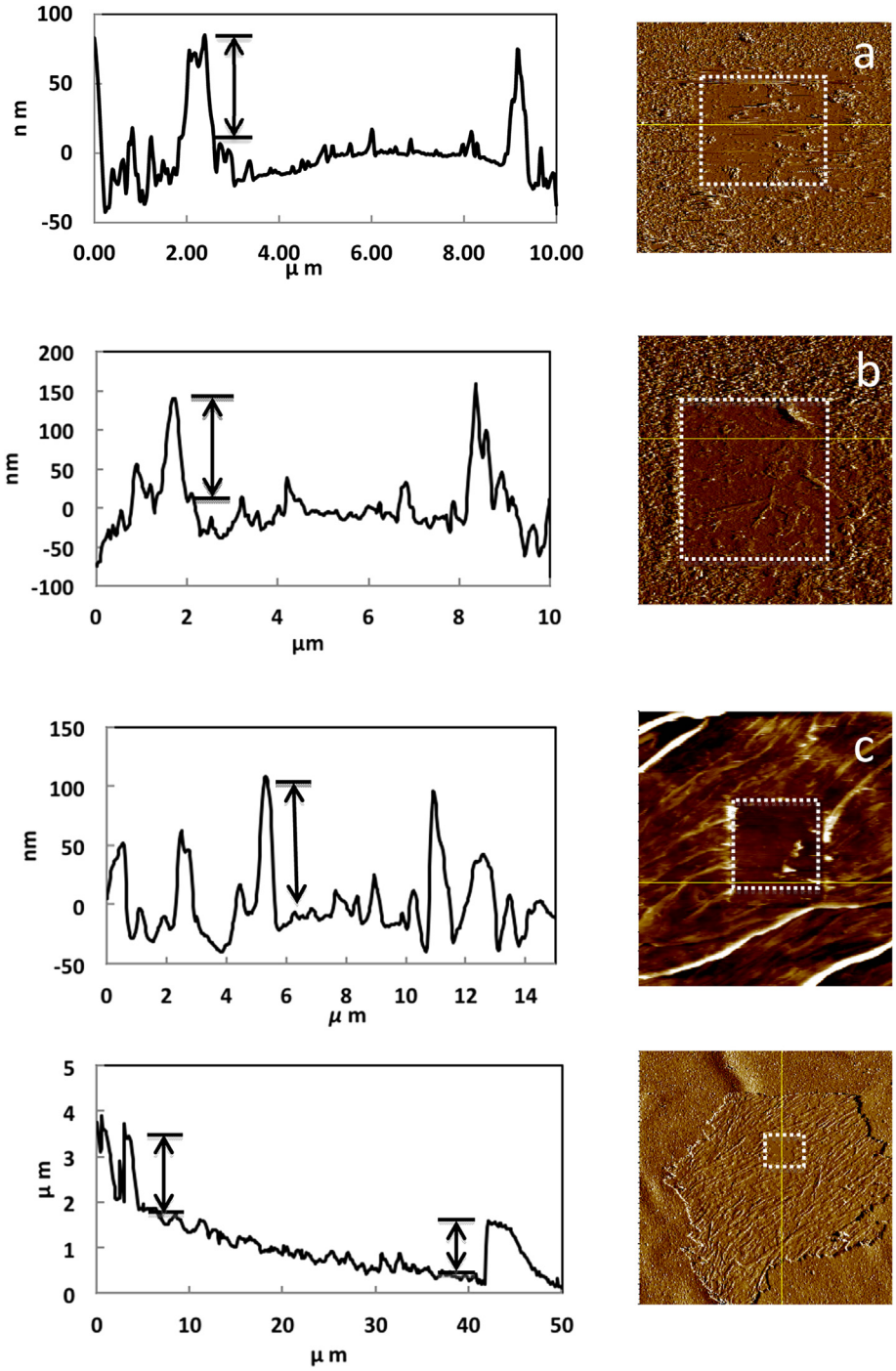

Fig. 6. Thickness of SEI layers during cycling. a)–b) Scan area 100 μm^2; c) 225 μm^2; d) 2500 μm^2.

voltage of 1.7 V. The swellings apparently move further into the HOPG edge with the lower discharge voltage (as shown in the white cycle in Fig. 4c and d). The exfoliation of the first particle layer can be attributed to the swelling of the bottom layer or the burst of the gas bubble formed during cycling as reported by Zeng et al. in their in-situ TEM study of SEI formation [16]. It can also be observed that the swelling bottom layer pushes the top particle layer off as a whole piece rather than crack the top layer. This is probably due to the higher interlayer integrity in the top particle layer compared to the van der Waals forces between the top layer and the bottom layer.

As schematically shown in Fig. 5, solvent decomposition products (designated with purple dots) form at the surface of the graphite electrode, corresponding to Fig. 5a. At a discharge voltage of 1.7 V, these particles loosely attach to the sample surface and do not show any preferences to the edge of the HOPG step, suggesting van der Waals forces rather than chemical bonds may be in effect.

Below the top particle layer, intercalation of solvated lithium ions (designated with gray dots) into the graphene layers takes place at the discharge voltage of 1.7 V (Fig. 5b), where the edge of HOPG and some spots at the basal plane show swelling due to the intercalation (white lines and dots observed in Fig. 4b). Note that

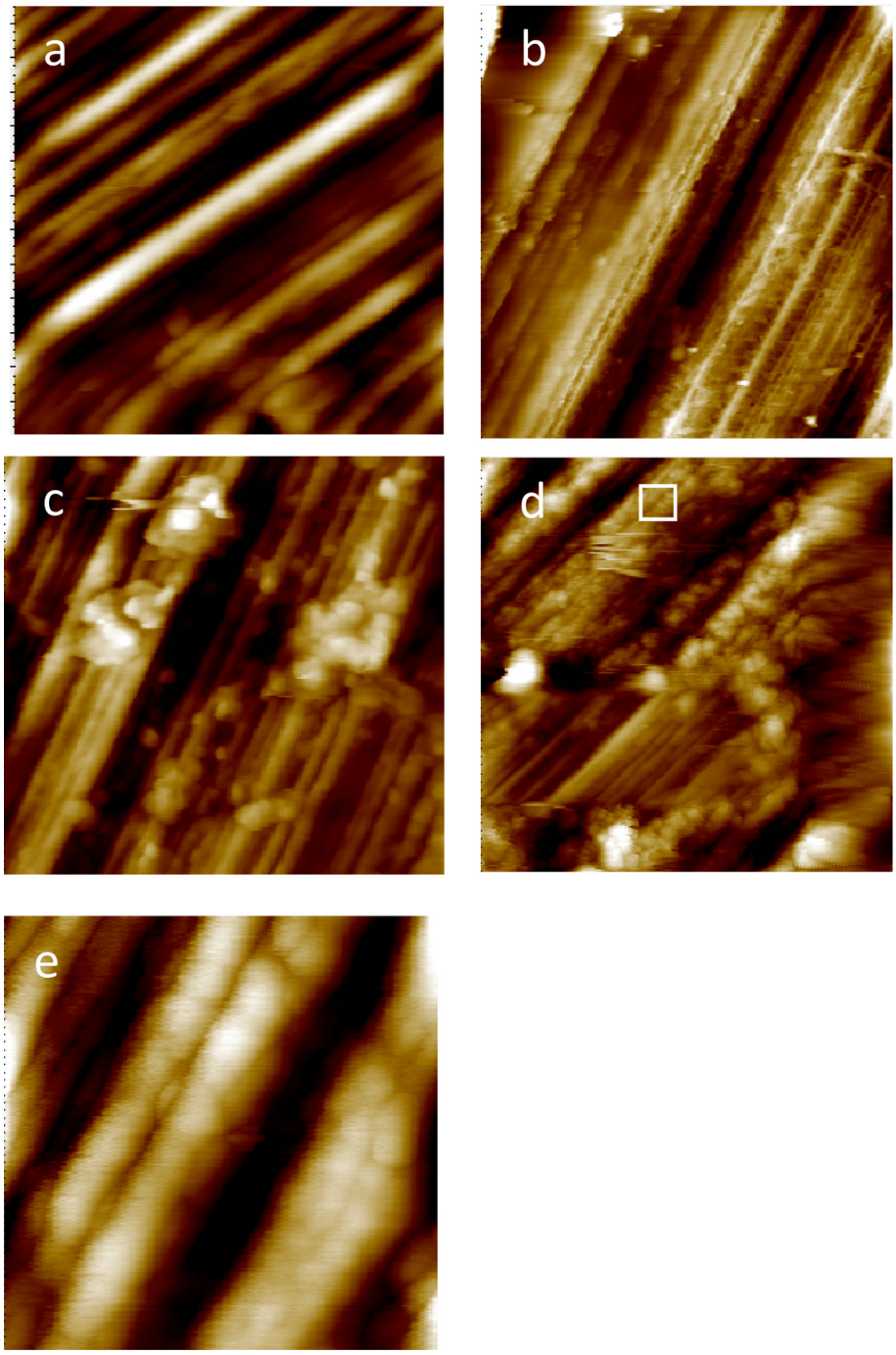

Fig. 7. AFM images of the graphite surface a) before cycling; b) after the first discharge process; c) after the first cycle; d) after the third cycle; e) zoom in image of d). a)–d) Scan area 25 μm^2; e) scan area 1.56 μm^2.

the hexagonal graphene unit cell (a:c = 1:2.73) space group $P6_3/mmc$ consists of layers of closely packed carbon atoms with relatively weak interlayer bonds (Fig. 5e). The solvated lithium ions can more easily overcome the graphene interlayer bonds than the covalent bonds within the graphene layers. Therefore, the intercalations are more likely to happen at the edge plane (perpendicular to 001 plane) rather than on 001 plane. This causes the severe curling of the edges at the HOPG steps compared to the relatively mild swelling of the basal planes (Figs. 4c and 5c).

The number of particles on the top of the HOPG surface keeps growing during the discharge process (Figs. 3d and 5c), while more lithium ions intercalate into the graphene layer causing the basal plane to swell out and edges to curl up. At the discharge voltage close to 0.02 V, the displaced curling edges mechanically push the particle layer off the HOPG surface. As shown in Fig. 3e and illustrated in Fig. 5d, the particle layers peel off as a sheet rather than crack on the surface, indicating that these particles are possibly held together by chemical bonds or inter-weaving of solvent decomposition products, which is stronger than van der Waals forces between the particle layer and HOPG surface. The swelling and the exfoliating at the HOPG surface are possible reasons for the electrode pulverization that causes the battery performance to

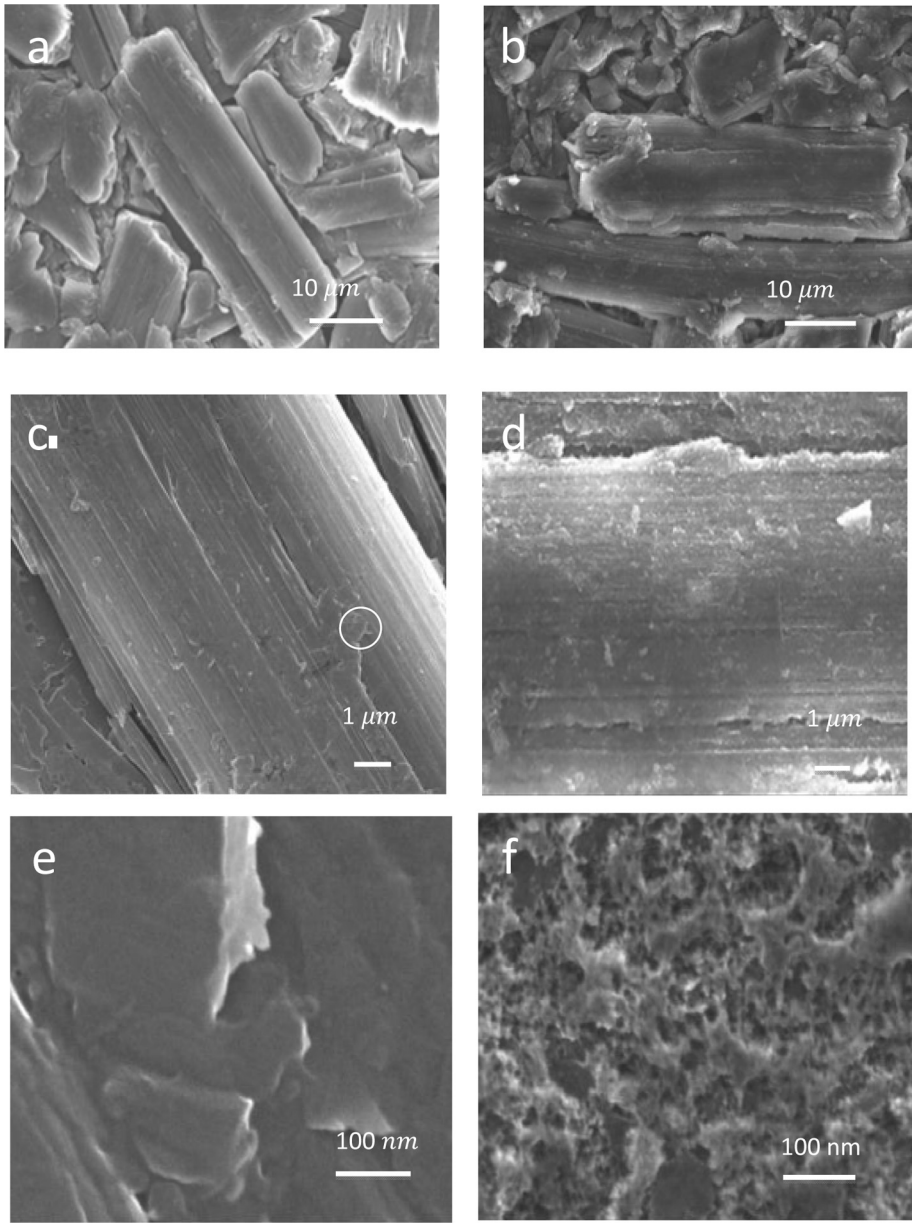

Fig. 8. SEM images of the graphite electrode before and after cycling. a) Pristine graphite composite electrode (×2000); b) graphite composite electrode after 8 cycles (×2000); c) pristine graphite composite electrode (×10,000); d) graphite composite electrode after 8 cycles (×2000); e) pristine graphite composite electrode (×200,000); f) graphite composite electrode after 8 cycles (×200,000).

decay. Thus, more edge planes than basal planes may be beneficial for lithium intercalations; HOPG with optimized strip width and percentage of edge planes is preferable to prevent drastic displacement and the exfoliation of the SEI layer.

Based on the discussion above, a dynamic competition SEI formation process involves the competition between the growth of the top particle layer and the bottom layer, as well as the inter reaction of these two layers. The top particle layer needs to be kept at a certain thickness to prevent the further solvent decomposition; however, it can also block the lithium ion pathways when it is thick and dense enough because lithium ions have to pass through the top particle layer first before intercalation into the HOPG surface. Therefore, the top layer needs to be controlled at a certain thickness and density to allow the lithium ion through. At the same time, the lithium insertion to the HOPG surface, as the major contribution to the cell capacity, needs to be maximized within a certain range where the insertion is not too much to cause the curling of the edges and pushing off the top layer. The SEI formation is considered as a dynamic competition of solvent decomposition, lithium insertion, pathway of lithium ion and attachment of the top particle layer to the HOPG surface.

3.3. Growth of SEI during cycling

Synchronous AFM probe scanning and cyclic voltammetry are performed to investigate the growth of the SEI layer. The depths of the SEI layers are examined by scratching a square (marked in the dotted white lines in Fig. 6) on the surface by using a 5 V force repeatedly on the probe. Then, a larger area that includes the dent is scanned to determine the thickness of the SEI layer. As it is shown in Fig. 6a, the depth of the SEI layer at 1.7 V during the first discharge cycle is around 80 nm. The SEI layer at this stage is

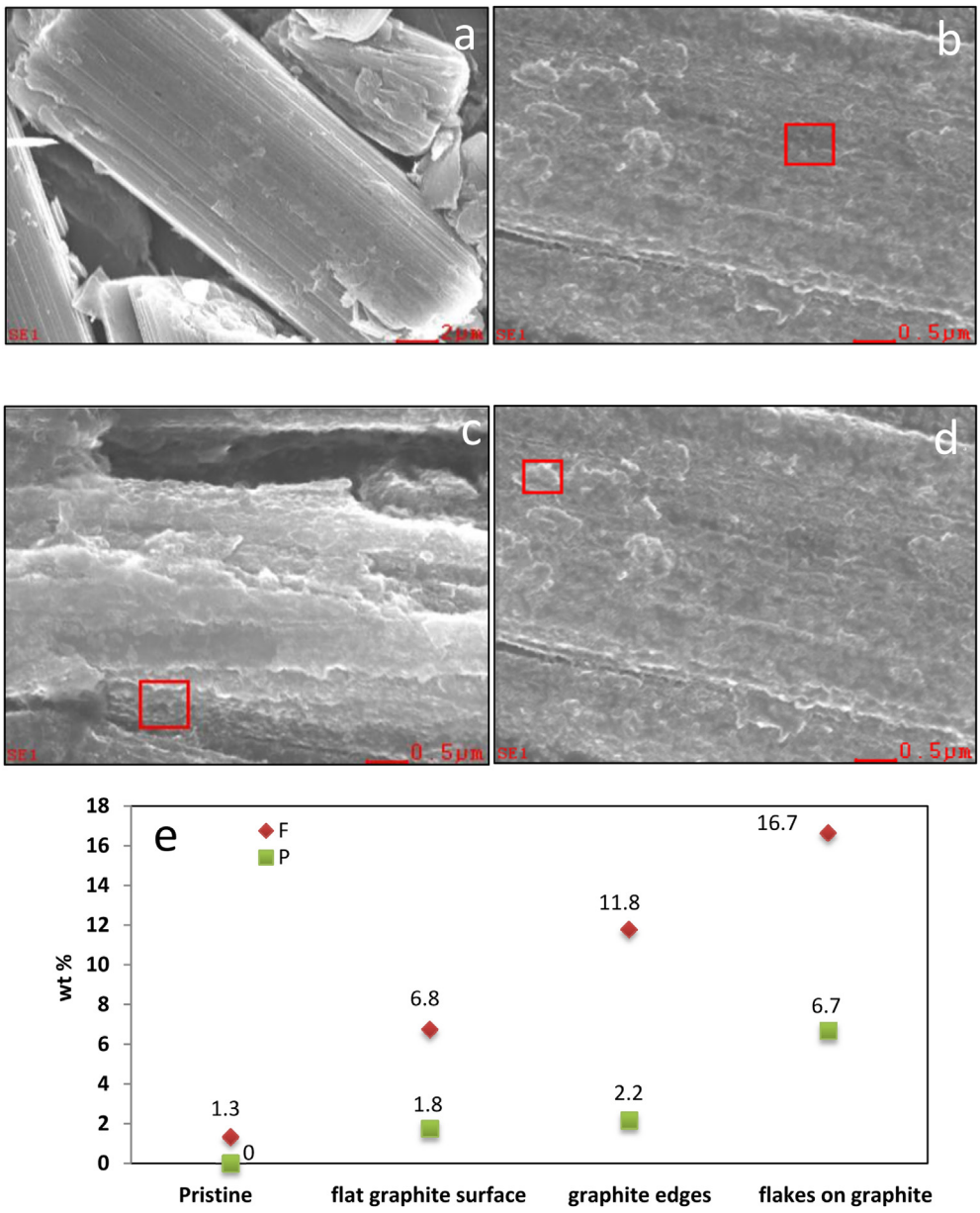

Fig. 9. FESEM and EDS analysis of the graphite rod surface before and after cycling, at different locations of the graphite rod. a) Pristine graphite rod; b) the flat surface on the graphite rod after 8 cycles; c) the edges of the graphite rod after 8 cycles; d) the flakes on the surface of graphite rod after 8 cycles; and e) the weight ratio of fluorine and oxygen in the pristine and cycled sample at different locations of the graphite rod. The red squares in b)–d) indicate the area where the EDS data were taken. (For interpretation of the references to color in this figure legend, the reader is referred to the web version of this article.)

still separated particles. The depth of this top particle layer increases accordingly as more particles are formed during the charging process, finally covering the entire HOPG surface. As shown in Fig. 6b, the depth of the top layer increased to about 120 nm at a voltage of 0.95 V after the discharge peak. In order to examine the depth that lithium ions can penetrate into HOPG surface, the top particle layer was completely scratched off, then a 5 × 5 micron dent was dug until the flat HOPG surface is observed. As shown in Fig. 6c, the thickness of SEI caused by lithium insertion is around 100 nm by the end of the first discharge process. By the end of the eighth cycle, the thickness increased to around 1.5 μm as shown in Fig. 6d. The thickness after the first discharge process here was very different than the 20–40 nm that Inaba et al. reported [4].

3.4. Morphology changes of the graphite composite electrode during cycling

The graphite composite electrode is also studied in order to understand the formation of SEI layers in a system similar to that of a commercial battery. The pristine graphite electrode is shown in Fig. 7a. The pristine sample has very definite strips of graphite with clear edges and resembling rods. However, the clear edges become blurry after the first discharge process, indicating that the insertion of the Li ions is happening at the edges (Fig. 7b). There are also small round particles with a diameter of about 100 nm observed after first discharge as shown in Fig. 7b. Clusters of these particles around 2 μm in diameter, formed during cycling, have been observed after the first cycle of charge and discharge (Fig. 7c). The

graphite strips are almost covered by these particles after 3 cycles, suggesting the growth of the SEI layer during cycling. Fig. 7e, which is a magnification of Fig. 7d, shows that the graphite strips are all covered with particles or particle clusters of around tens of nanometers across as well.

Compared to the HOPG surface, there is no obvious exfoliation at the edge of the graphite composite electrode. This is probably because the graphite composite electrode is composed of thin strips of 200–400 nm in diameters, into which lithium ions are able to penetrate from both sides of the edges all the way into the center. Therefore, both the center and the edges swell up at the same time rather than only the edges swell in the case of HOPG surface due to the lack of edge planes. Therefore, the top particle layer observed still covers the graphite after 3 cycles on the graphite composite electrode.

4. Ex-situ field emission scanning electron microscopy characterization

The morphologies of the pristine electrode and the electrode after 8 cycles were characterized using FESEM. Graphite rods are observed on the surface with diameters from 10 μm to 15 μm and lengths ranging over several tens of micrometers. Small particles and flakes around 10 microns or less are also found between the graphite rods (Fig. 8a). Irregular flakes of about 100 nm can also be observed on the surface of the graphite rods in Fig. 8a (shown in white cycles).

The graphite rods appear to be more fractured after 8 cycles of charge and discharge. They display a looser and more blurry texture and more obvious ribbons on the surface compared to the graphite rods of the pristine electrode surface. The edge of the ribbons on the surface of the graphite rods becomes less distinct after 8 cycles (Fig. 8b). Occasionally, porous structures with a pore size of 10–20 nm can be found on the surface of graphite rods (Fig. 8f), compared to the pristine graphite rod (Fig. 8e). The nanosized pores are believed to be formed by the escaping gas generated by the decomposition of lithiated solvent between the graphene layers [17,18].

5. Ex-situ energy dispersive X-ray spectrometry (EDS) characterization

In order to further investigate the components of the SEI layer, the graphite electrode before and after cycling was characterized by EDS. As seen in Fig. 9a and e, fluorine and oxygen weight ratios in the pristine sample are 4.8% and 1.3% on the graphite rod surface. The fluorine and oxygen weight ratio on the flat part of graphite rod surface after 8 cycles shows an increase to 6.8% and 1.8%, respectively (Fig. 9b and e). However, drastic increases of the fluorine and oxygen contents were observed at the edge (11.8% and 2.2%) of the graphite rod and the flakes (11.9% and 2.9%) on the surface of the rod as shown in the red squares in Fig. 9c, d and e. This is in good agreement with what was observed in in-situ AFM images, where we concluded that the lithium intercalation happens mostly at the edge planes rather than at the basal planes due to its interlayer bonds being weaker than the covalent bonds within the graphene layer. However, residues of solvent decomposition and lithiation were also observed at the flat surface, revealing that the solvated lithium ion might be capable of penetrating from the 001 plane into the graphene layers.

6. Conclusions

Current work elucidated SEI evolution during cell cycling. Based on the conducted study, a dynamic competition mechanism for increase in SEI thickness has been proposed. SEI layer formation and evolution on a model material (highly oriented pyrolytic graphite, HOPG) surface during the first discharge process has been investigated by in-situ AFM technology. The morphology changes of both the top particle layer and the bottom lithium intercalation layer are observed for the first time. The top particle layer of the SEI forms at around 1.7 V. The thickness of this layer grows from a single layer of approximately 200 nm thick to about 1.5 μm at the end of the 8th cycle. The particle size at the end of the 8th cycle reaches 100 nm. Despite reported in many papers that SEI formation happens in the first charge–discharge cycle, it is observed in this study that the thickness and particle size of the top SEI layer keeps growing even after 8 charge–discharge cycles. The irreversible formation of the particle layer, which can be attributed to the decomposition products of the electrolyte, does not contribute to the capacity. The bottom SEI layer, on the other hand, is more likely to be the functional SEI layer in the charging process.

A graphite composite electrode that is close to what would be found in a real battery system is also investigated. The similar swelling phenomenon at the edge during Li inserting is observed for a graphite composite electrode. Furthermore, ex-situ FESEM and EDS are used to help understand the morphology and compositions after cycling. The percentages of SEI residues (indicated by wt% of F and O) on both the edges and the surface flakes of the graphite composite electrode increase drastically after cycling. These results of the FESEM and EDS experiments are in good agreement with the observed phenomenon and proposed mechanism based on the in-situ AFM experiments. The study on graphite composite electrode further illustrates that layered electrode surface provides more reaction sites compared to flat HOPG surface.

Acknowledgement

Financial support from General Motors Company and the Department of Energy (Grant DEFG36-05GO85005) for this research is gratefully acknowledged. In addition, we would like to thank Dr. Song Xu from Agilent Technologies for his assistance on the setup of in-situ AFM cell and trouble-shooting on AFM operation, and Dr. Mark Cheng, Department of Electrical Engineering, Wayne State University, for the use of AFM to acquire part of the in-situ AFM data.

References

[1] I. Lucas, E. Pollak, R. Kostecki, Electrochem. Commun. 11 (2009) 2157–2160.
[2] Q.P. McAllister, K.E. Strawhecker, C.R. Becker, C.A. Lundgren, J. Power Sources 257 (2014) 380–387.
[3] A. Tokranov, B.W. Sheldon, C. Li, S. Minne, X. Xiao, Appl. Mater. Interfaces (2014). Forthcoming.
[4] M. Inaba, S.K. Jeong, Zempachi Ogumi, Interface 20 (2011) 55–59.
[5] E.P. Campana, J. Vetter, P. Navak, H. Siegenthaler, Electrochem. Commun. 7 (2005) 107–112.
[6] F.M. Loster, D.A. Scherson, J. Phys. Chem. B 110 (2006) 18081–18087.
[7] S.K. Jeong, R. Mogi, Y. Iriyama, T. Abe, Z. Ogumi, J. Power Sources 17 (2001) 119–121.
[8] S. Kalinin, N. Balke, S. Jesse, A. Tselev, A. Kumar, T.M. Arruda, S. Guo, R. Proksch, Mater. Today 14 (2011) 548–558.
[9] S.K. Jeong, M. Inaba, Y. Iriyama, T. Abe, Z. Ogumi, J. Power Sources 119 (2003) 555–560.
[10] Y.S. Cohen, D. Aurbach, Electrochem. Commun. 6 (2004) 536–542.
[11] Agilent AFM 5500 User Manual.
[12] D. Aurbach, Y. Ein-Eli, O. Chusid (Youngman), Y. Carmeli, M. Babai, H. Yamin, J. Electrochem. Soc. 141 (1994) 603–611.
[13] D. Aurbach, B. Markovsky, I. Weissman, E. Levi, Y. Ein-Eli, Electrochim. Acta 45 (1999) 67–86.
[14] D. Bar-Tow, E. Peled, L. Bursteinb, J. Electrochem. Soc. 146 (1999) 824–832.
[15] S. Mori, H. Asahina, H. Suzuki, A. Yonei, K. Yokoto, J. Power Sources 68 (1997) 59–64.
[16] Z. Zeng, W. Liang, H. Liao, H.L. xin, Y. Chu, H. Zheng, Nano Lett. 14 (2014) 1745–1750.
[17] G. Eichinger, J. Electroanal. Chem. 74 (1976) 183–193.
[18] A.N. Dey, B.P. Sullivan, J. Electrochem. Soc. 117 (1970) 222–224.